J. Fluid Mech. (2001), *vol.* 444, *pp.* 23–47. Printed in the United Kingdom

On the slow draining of a gravity current moving through a layered permeable medium

By DAVID PRITCHARD[1], ANDREW W. WOODS[2] AND ANDREW J. HOGG[1]

[1]Centre for Environmental and Geophysical Flows, School of Mathematics, University of Bristol, University Walk, Bristol BS8 1TW, UK

[2]BP Institute, University of Cambridge, Madingley Rise, Madingley Road, Cambridge CB3 0EZ, UK

(Received 11 April 2000 and in revised form 6 March 2001)

We examine the gravitational dispersal of dense fluid through a horizontal permeable layer, which is separated from a second underlying layer by a narrow band of much lower permeability. We derive a series of analytical solutions which describe the propagation of the fluid through the upper layer and the draining of the fluid into the underlying region. The model predicts that the current initially spreads according to a self-similar solution. However, as the drainage becomes established, the spreading slows, and in fact the fluid only spreads a finite distance before it has fully drained into the underlying layer. We examine the sensitivity of the results to the initial conditions through numerical solution of the governing equations. We find that for sources of sufficiently large initial aspect ratio (defined as the ratio of height to length), the solution converges rapidly to the initially self-similar regime. For longer and shallower initial source conditions, this convergence does not occur, but we derive estimates for the run-out length of the current, which compare favourably with our numerical data. We also present some preliminary laboratory experiments, which support the model.

1. Introduction

There are numerous industrial and natural situations in which liquid spreads through a layered porous medium. For example, many sedimentary deposits are composed of numerous laterally continuous layers, of different grain sizes and hence different permeabilities and which are associated with different phases of sedimentation. In some situations, an intruding fluid flow is driven by the gravitational forces associated with the density differences between the fluid in the current and the host fluid in the reservoir. Important examples involve displacement flows in oil reservoirs, in which an injectate, such as polymer-laden water, displaces oil through the reservoir (Christie & Blunt 1993; Lake 1989), water injection in geothermal reservoirs (Woods 1999), and the dispersal of pollutants through groundwater (Bear 1972). The dynamics of such currents may be complex, particularly in displacement flows, owing to the effects of viscosity contrasts, capillary forces, wettability of the porous matrix, and small-scale heterogeneities in the reservoir. These effects often lead to the formation of a zone in which the two fluids mix. However, when the buoyancy force associated with a density difference between the fluids dominates the motion, and the viscosity contrast does not lead to a fingering instability, the interface may remain relatively well-defined and sharp compared to the overall scale of the flow (e.g. Woods & Mason

2000). In such a situation, it is of interest to develop a macroscopic picture of the displacement of the interface between the two fluids, as a leading-order approximation for the flow.

In this paper, we examine the motion of a gravity-driven flow propagating through a permeable medium. We focus on flow through a horizontal layer of high permeability, accounting for the effect of the drainage of some fluid through a thin underlying layer of smaller permeability and into a second high-permeability layer. This is a simplified picture of flow in a complex layered medium, but illustrates the important role of the draining flow in limiting the lateral propagation of the current.

Our model is complementary to the recent experimental work of Thomas, Marino & Linden (1998) and the analytical work of Ungarish & Huppert (2000), which investigate the effect of drainage on an inertial gravity current. Their models share some features with ours, such as the finite run-out distance, but because of the greater dynamical complexity of the system which they consider, they were only able to obtain analytical solutions for a simplified 'box' model. Our model also complements the work of Davis & Hocking (1999, 2000), which considers the spreading of viscous liquid on a porous base into which it drains. However, capillary effects are an essential component of Davis & Hocking's model, whereas we are able at the macroscopic scale to ignore them.

We account for two distinct forms of drainage into the base. The first corresponds to gravity-driven drainage and the second corresponds to drainage driven by a uniform background vertical flow. This latter model also describes a gravity-driven particle-laden flow through a fracture, in which the volume of relatively dense fluid in the current decreases as a result of particle sedimentation. After presenting a series of particular analytical solutions for these models (§ 2), we conduct some numerical experiments to examine the sensitivity of these solutions to the detailed initial conditions (§ 3). In § 4, we describe preliminary results from analogue laboratory experiments. Finally, in § 5 we discuss the significance and application of our results.

2. Models of draining gravity currents

First, we review the motion of an intruding current of relatively dense fluid along an impermeable bed, in a planar geometry. We then extend this to situations in which the bed is permeable, and the denser fluid drains into the bed under the effects of gravity (§ 2.2) or an imposed background flow (§ 2.3). Finally, in § 2.4, we extend this further, to an axisymmetric current. We note that our models will also describe the motion of an intruding current of buoyant fluid along an upper boundary, though for convenience we restrict ourselves in this paper to the case of denser intruding fluid.

The model flow is illustrated in figure 1. We examine the motion of liquid of density $\rho + \Delta\rho$ and viscosity μ through a porous layer of permeability K and porosity ϕ, which is saturated with liquid of density ρ. The bed of the layer is assumed to have permeability $K_b (\ll K)$ and porosity ϕ_b.

In each case, the current is assumed to be long and thin, so that the aspect ratio $H/L \ll 1$, where L is the length, and H a typical depth, of the current. Under this assumption, motion in both the current and the ambient is, to first order in H/L, unidirectional and parallel to the bed, and so the pressure can be assumed to be hydrostatic (e.g. Huppert & Woods 1995). The pressure within the current is then given by

$$p = p_0 + \Delta\rho g(h - y) + \rho g(H_a - y), \quad h > y > 0, \tag{2.1}$$

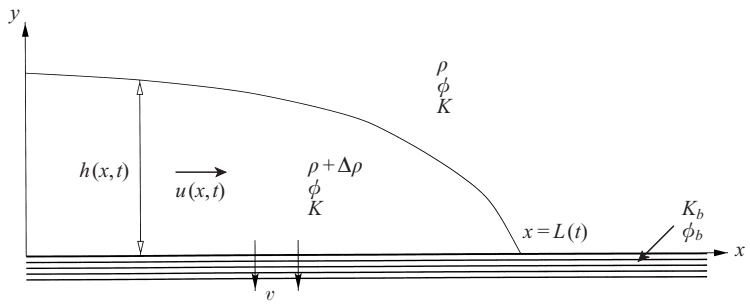

FIGURE 1. Definition diagram for gravity current through porous medium with a permeable bed.

where p_0 is an arbitrary constant pressure at the top of the porous layer, g is gravitational acceleration, and H_a is the depth of the layer.

We further assume that the depth of the ambient fluid is large compared to that of the current, $H_a \gg H$, so we may neglect the effect of any return flow. (When the depth of the ambient fluid is comparable to that of the current, the problem becomes similar to that of a reservoir exchange flow (Huppert & Woods 1995), modifying both the shape and the motion of the interface.)

In this approximation, the continuity equation has the form

$$\phi \frac{\partial h}{\partial t} + \frac{\partial}{\partial x}(uh) = 0, \tag{2.2}$$

where u is the horizontal transport velocity in the current.

Finally, the transport velocity is modelled by Darcy's law for low Reynolds number flow through a permeable medium,

$$u = -\frac{K}{\mu}\frac{\partial p}{\partial x}. \tag{2.3}$$

2.1. *Impermeable base (no drainage)*

In the limit $K_b = 0$, corresponding to an impermeable underlying boundary, there is no drainage of fluid into the bed, and the volume of fluid in the permeable layer is conserved. We follow Huppert (1986) to obtain a similarity solution for the shape of the current.

Combining (2.3) with (2.2), we obtain the governing equation

$$\frac{\partial h}{\partial t} = \beta \frac{\partial}{\partial x}\left(h \frac{\partial h}{\partial x}\right), \tag{2.4}$$

where

$$\beta = \frac{Kg\Delta\rho}{\mu\phi}. \tag{2.5}$$

For the subsequent discussion, a useful reference case concerns the motion of an instantaneous release of a finite volume per unit width of relatively dense fluid. We define the volume per unit width to be $V(t) = \int_0^L h(x,t)\,\mathrm{d}x$, where $L(t)$ is the length of the current. For a non-draining current, this will be constant, $V(t) = \mathscr{V}$, and for a draining current, we will define $\mathscr{V}$ to be the initial volume per unit width of the current, $\mathscr{V} = \lim_{t\to 0} V(t)$. Some natural dimensionless variables can now be defined,

$$\hat{x} = \frac{x}{\mathscr{V}^{1/2}}, \quad \hat{t} = \frac{t\beta}{\mathscr{V}^{1/2}}, \quad \hat{h} = \frac{h}{\mathscr{V}^{1/2}}, \tag{2.6}$$

giving the governing equation the form

$$\frac{\partial \hat{h}}{\partial \hat{t}} = \frac{\partial}{\partial \hat{x}}\left(\hat{h}\frac{\partial \hat{h}}{\partial \hat{x}}\right). \tag{2.7}$$

The global conservation of volume requires that $\int_0^{\hat{L}} \hat{h}(\hat{x},\hat{t})\,\mathrm{d}\hat{x} = 1$, and the no-flux condition at $\hat{x} = 0$ gives $\partial\hat{h}/\partial\hat{x} = 0$ at $\hat{x} = 0$. This problem has the classic exact similarity solution (Pattle 1959)

$$\hat{h}(\hat{x},\hat{t}) = \tfrac{1}{6}\hat{t}^{-1/3}\left(9^{2/3} - \frac{\hat{x}^2}{\hat{t}^{2/3}}\right). \tag{2.8}$$

We note that the solution (2.8) corresponds formally to an initial condition where the fluid is concentrated at the origin at $t = 0$. This clearly does not represent a realistic distribution of fluid, and in fact violates the assumption of small aspect ratio on which the model was based. However, (2.8) is also known (Barenblatt 1996) to act as an 'intermediate asymptotic' for solutions with a more general class of initial conditions. This is discussed further in § 3.

2.2. *Gravity-driven drainage*

We now consider how the flow evolves if the base of the high-permeability layer consists of a thin layer of permeability K_b ($\ll K$) and thickness b ($\ll H$), beneath which there is a further relatively deep high-permeability channel. This picture is characteristic of a number of sedimentary deposits in which a thin low-permeability, clay-rich deposit may form between two higher-permeability layers.

Since the low-permeability layer is very thin, a small vertical flow may develop through this layer, dominated by the gravitational head of the overlying current relative to that in the surrounding fluid. We consider the regime in which the time of drainage across this layer, $t_d \sim (\nu b^2)/(K_b g' h)$, is much smaller than the time for flow along the high-permeability layer, $t_f \sim (\nu L)/(K g'(\partial h/\partial x))$ (where $\nu = \mu/\rho$, $g' = g\Delta\rho/\rho$). This requires $L \gg (K/K_b)^{1/2} b$: under this condition, the vertical volume flux per unit area through the lower layer is given by

$$v = -\frac{K_b}{\mu}\frac{\Delta\rho g h}{b}. \tag{2.9}$$

This flow continues downwards through the thin layer of low permeability and into the underlying layer of much higher permeability. Owing to the contrast in permeability, the pressure gradients associated with the flow below the thin layer are negligible. The process of drainage modifies the equation for the conservation of mass in the main current (in the upper high-permeability channel) to the form

$$\phi\frac{\partial h}{\partial t} = -\frac{\partial}{\partial x}(uh) - v. \tag{2.10}$$

Combining these equations, we find that the governing equation for the flow takes the form

$$\frac{\partial h}{\partial t} = \beta\frac{\partial}{\partial x}\left(h\frac{\partial h}{\partial x}\right) - \beta\frac{K_b}{K}\frac{h}{b}, \tag{2.11}$$

where β is defined by equation (2.5). Equation (2.11) is a generalization of the nonlinear diffusion equation (2.7) for a current spreading along an impermeable boundary, which now accounts for the drainage of the flow.

We note in passing that for a current supplied by a source of fluid $Q(t)$ and with the extent of the current given by $L(t)$, we can obtain a simple expression for the global conservation of mass of dense fluid in the current,

$$\frac{\mathrm{d}V(t)}{\mathrm{d}t} = Q(t) - \beta\frac{K_b}{bK}V(t), \tag{2.12}$$

which indicates that the volume of the current per unit width evolves according to the relation

$$V(t) = \exp\left(-\beta\frac{K_b t}{bK}\right)\left[V(0) - \int_0^t Q(t')\exp\left(\beta\frac{K_b t'}{bK}\right)\mathrm{d}t'\right]. \tag{2.13}$$

2.2.1. *Finite-volume release*

For comparison with the case of an impermeable lower boundary, described in § 2.1, we now examine the motion of a finite volume of fluid $\mathscr{V}$ per unit width, released at $t = 0$. As in § 2.1, we can introduce dimensionless variables (2.6), so that equation (2.11) reduces to the form

$$\frac{\partial\hat{h}}{\partial\hat{t}} = \frac{\partial}{\partial\hat{x}}\left(\hat{h}\frac{\partial\hat{h}}{\partial\hat{x}}\right) - \lambda\hat{h}, \tag{2.14}$$

where $\lambda = (K_b\mathscr{V}^{1/2})/(Kb)$. The dimensionless parameter λ represents the ratio of the horizontal to vertical velocity scales, assumed to be much less than unity.

Equation (2.14) can be transformed to the original nonlinear diffusion equation (2.7) using the substitutions (see e.g. Murray 1989)

$$H = \hat{h}\exp(\lambda\hat{t}) \quad \text{and} \quad \tau = \frac{1-\exp(-\lambda\hat{t})}{\lambda}, \tag{2.15}$$

so that

$$\frac{\partial H}{\partial\tau} = \frac{\partial}{\partial\hat{x}}\left(H\frac{\partial H}{\partial\hat{x}}\right). \tag{2.16}$$

As in § 2.1, this has solution

$$H = \tfrac{1}{6}\tau^{-1/3}\left(9^{2/3} - \frac{\hat{x}^2}{\tau^{2/3}}\right). \tag{2.17}$$

Figure 2 shows a numerical experiment in which this solution was reproduced using the numerical method described in Appendix A. The overall pattern of the motion involves an initial spreading phase, followed by a drainage-dominated phase. The nose of the current has position

$$\hat{L}(\hat{t}) = 9^{1/3}\tau^{1/3} = \left[\frac{9}{\lambda}(1-\exp[-\lambda\hat{t}])\right]^{1/3}. \tag{2.18}$$

This illustrates how, as the flow evolves from the spreading phase into the draining regime, the current approaches the maximum lateral extent $(9/\lambda)^{1/3}$.

2.2.2. *Steady-flow solution*

With a steady supply of fluid at $x = 0$, the flow regime is somewhat different. A steady state becomes possible in which the drainage flux matches the source flux. If we denote the constant flux by $\mathscr{Q}$, and introduce the dimensionless length and time scales $\mathscr{Q}/\beta$ and $\mathscr{Q}/\beta^2$ respectively, where β is defined by equation (2.5), then we obtain

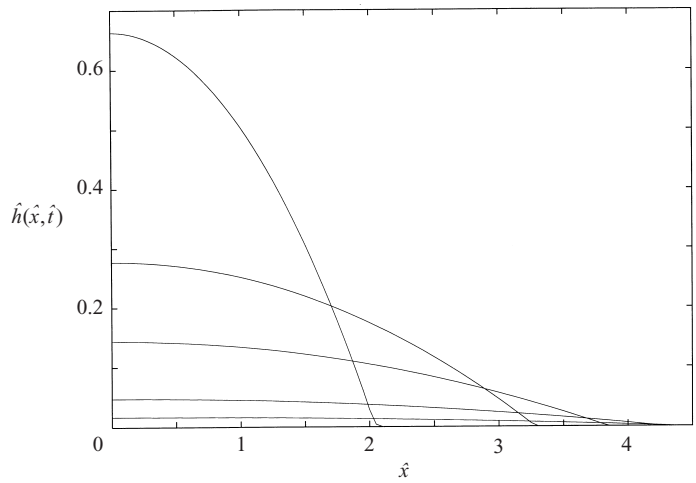

FIGURE 2. Analytical solution for gravity-driven drainage with $\lambda = 0.1$: height of the current, $\hat{h}$, as a function of distance $\hat{x}$, at $\hat{t} = 1, 5, 10, 20, 30$. Note the run-out length $\hat{L}_\infty = (9/\lambda)^{1/3} \approx 4.48$.

an equation governing the steady shape of the current:

$$\frac{\mathrm{d}}{\mathrm{d}\hat{x}}\left(\hat{h}\frac{\mathrm{d}\hat{h}}{\mathrm{d}\hat{x}}\right) = \lambda_{\mathscr{Q}}\hat{h}, \tag{2.19}$$

with $\lambda_{\mathscr{Q}} = (K_b\phi\mathscr{Q})/(K\phi_b b\beta)$.

For this steady flow, the flux boundary condition at the origin has the form $h(0)u(0) = \mathscr{Q}$, which may be expressed as $\hat{h}(\partial\hat{h}/\partial\hat{x}) = -1$ at $\hat{x} = 0$. With this boundary condition, equation (2.19) has steady solution

$$\hat{h}(\hat{x}) = \frac{\lambda_{\mathscr{Q}}}{6}\left[\hat{x} - \left(\frac{18}{\lambda_{\mathscr{Q}}^2}\right)^{1/3}\right]^2. \tag{2.20}$$

Figure 3 shows a numerical experiment where the time-dependent equation 2.14 was solved with constant unit flux and with $\lambda_{\mathscr{Q}} = 0.5$, illustrating how the flow evolves towards this solution from a triangular initial shape. The current approaches a parabolic shape rapidly, and then gradually increases in length until it asymptotes to the analytical solution. A series of similar experiments suggest that this behaviour is typical.

2.3. *Drainage driven by background flow*

If there is an externally imposed uniform vertical background flow through the permeable rock, then as a dense current spreads along the high-permeability layer, a part of the fluid will drain into the underlying layer. We consider situations where the background pressure gradient drives a flow which is much greater than the drainage driven by the hydrostatic pressure within the current, but is still small compared to horizontal flows in the high-permeability layer. In this regime, the loss of fluid from the current now occurs at a constant volume flux per unit area, w, and the evolution becomes governed by the equation

$$\phi\frac{\partial h}{\partial t} = \frac{Kg\Delta\rho}{\mu}\frac{\partial}{\partial x}\left(h\frac{\partial h}{\partial x}\right) - w. \tag{2.21}$$

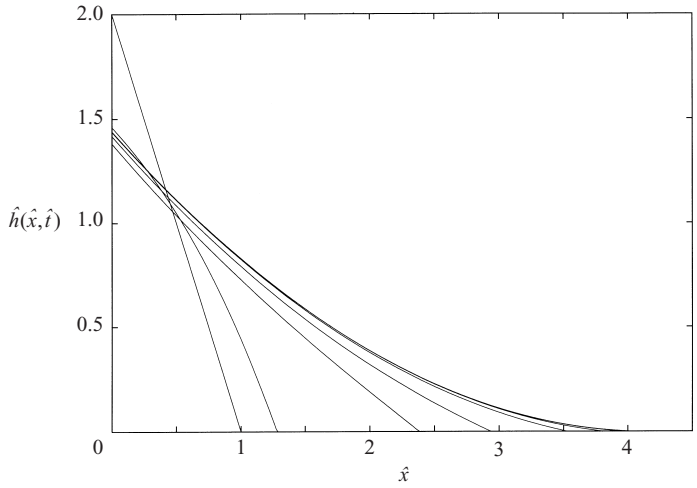

FIGURE 3. Profiles of current depth as a function of position, $\hat{h}(\hat{x},\hat{t})$, at the dimensionless times $\hat{t} = 0$, 0.15, 1.5, 3, 6, 9, 12, 15, showing the evolution to the steady-flow solution for $\lambda_2 = 0.5$.

In this case, there is no simple relation for the global conservation of mass, such as (2.13), since the evolution equation for the volume of fluid in the upper layer is not decoupled from the length of the current. However, the equation does admit an exact analytical solution, as described below.

It is interesting to note that equation (2.21) also describes the low Reynolds number gravity-driven flow of a particle-laden current propagating in a narrow crack (of width L_c), in which the density difference between the current and the ambient fluid arises from the particles. In this case (see Huppert 1986), the dynamics of the current without particle settling are described by

$$\frac{\partial h}{\partial t} = \frac{g' L_c^2}{12\nu} \frac{\partial}{\partial x}\left(h \frac{\partial h}{\partial x}\right). \tag{2.22}$$

The effects of particle settling may be described by including a term $-w_s$ on the right-hand side of equation (2.22) to represent the rate of release of fluid at the top of the current associated with the particle settling.

2.3.1. *Finite-volume release*

In the case of a finite-volume release, we can again use the scalings (2.6) to obtain a dimensionless equation governing the evolution of the current,

$$\frac{\partial \hat{h}}{\partial \hat{t}} = \frac{\partial}{\partial \hat{x}}\left(\hat{h} \frac{\partial \hat{h}}{\partial \hat{x}}\right) - \epsilon. \tag{2.23}$$

Here $\epsilon = w/\beta$ represents the ratio of the draining (or sedimenting) velocity to the horizontal velocity scale of the current. We have found an exact solution to equation (2.23), given by

$$\hat{h}(\hat{x},\hat{t}) = \tfrac{1}{6}\hat{t}^{-1/3}\left(9^{2/3} - \frac{\hat{x}^2}{\hat{t}^{2/3}}\right) - \tfrac{3}{4}\epsilon\hat{t}. \tag{2.24}$$

Figure 4 illustrates how this solution evolves with time: initially, the motion is very similar to that of the non-draining solution, but as the flow evolves, the effect of

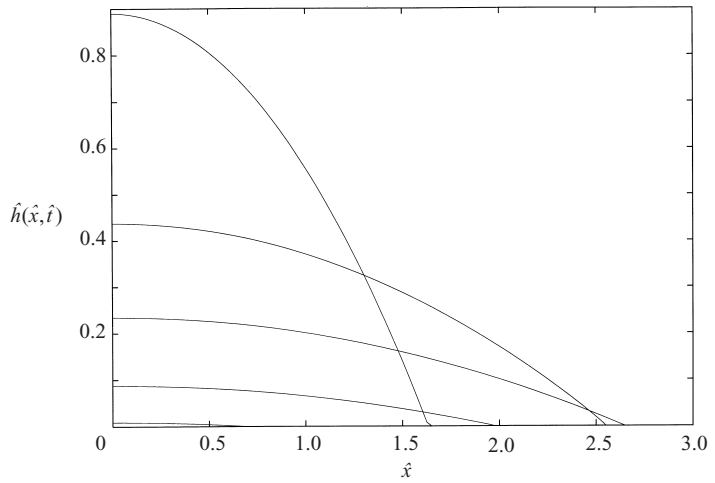

FIGURE 4. Analytical solution for drainage driven by background flow, with $\epsilon = 0.05$: height $\hat{h}$ as a function of $\hat{x}$ at $\hat{t} = 0.5, 2.5, 5, 7.5, 9$.

drainage into the lower less-permeable layer becomes dominant. This may be seen from the variation of the lateral extent of the current, $\hat{L}(\hat{t})$, with time,

$$\hat{L}(\hat{t}) = \hat{t}^{1/3}(9^{2/3} - \tfrac{9}{2}\epsilon\hat{t}^{4/3})^{1/2}. \tag{2.25}$$

$\hat{L}(\hat{t})$ in fact reaches a maximum length $\hat{L}_{\max} = (8/3)^{1/4}\epsilon^{-1/4}$, in a finite time $\hat{t}_{\max} = (8/243)^{1/4}\epsilon^{-3/4}$.

We note that, in the context of particle settling, the rate of fluid loss from the current is the sedimentation velocity w_s. Assuming that w_s is given by the Stokes settling velocity, it is inversely proportional to the kinematic viscosity ν of the interstitial fluid. Hence $\epsilon = w_s/\beta$ is independent of ν, and so the run-out length of the current is independent of the kinematic viscosity of the fluid. This is because an increase in viscosity decreases the vertical settling speed, but also reduces the horizontal spreading rate. The only effect of viscosity is to alter the dimensional time, $t_{\max} = \mathscr{V}^{1/2}\hat{t}_{\max}/\beta$, which it takes to reach this length.

Note also that the solution (2.24) can be rewritten in the form

$$\begin{aligned}\hat{h}(\hat{x},\hat{t}) &= \tfrac{1}{6}\hat{t}^{-1/3}(9^{2/3} - \tfrac{9}{2}\epsilon\hat{t}^{4/3})(1-\zeta^2)\\ &= \hat{h}(0,\hat{t})(1-\zeta^2),\end{aligned} \tag{2.26}$$

where $\zeta = \hat{x}/\hat{L}(\hat{t})$. We will refer to this in § 3.

2.3.2. *Steady-flow solution*

As in the case of the gravity-driven draining process (§ 2.2), it is also of interest to examine the steady-state solution which becomes established with a steady source of fluid at $x = 0$. If the volume flux per unit width supplied to the current at $x = 0$ is $\mathscr{Q}$, then the flow has length scale $\mathscr{Q}/\beta$ and time scale $\mathscr{Q}/\beta^2$, leading to the dimensionless equation

$$0 = \frac{\mathrm{d}}{\mathrm{d}\hat{x}}\left(\hat{h}\frac{\mathrm{d}\hat{h}}{\mathrm{d}\hat{x}}\right) - \epsilon, \tag{2.27}$$

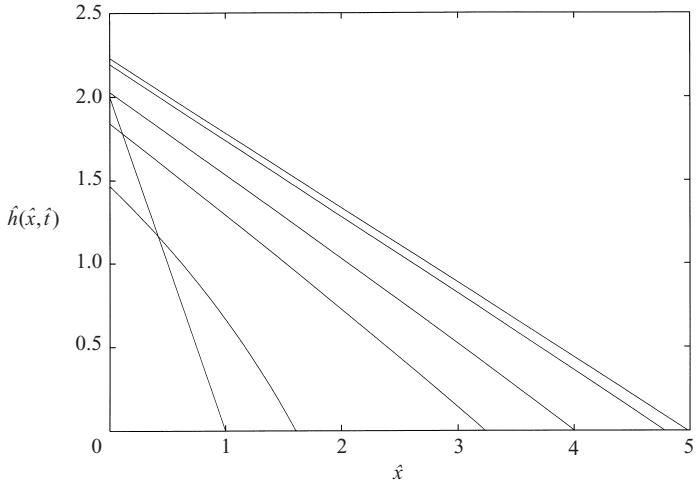

FIGURE 5. Current profile, $\hat{h}(\hat{x},\hat{t})$ as a function of $\hat{x}$ for $\hat{t} = 0$, 0.4, 4, 8, 20, 40, showing evolution to the steady-flow solution for $\epsilon = 0.2$.

with $\epsilon = w/\beta$ as before. If we apply the flux boundary condition at the origin, $\mathcal{Q} = u(0)h(0)$, and the global conservation of volume, $\mathcal{Q} = \epsilon L$, then we find the solution for the shape of the current:

$$\hat{h}(\hat{x}) = \frac{1}{\sqrt{\epsilon}}(1 - \epsilon\hat{x}). \tag{2.28}$$

This solution is obvious since, in the steady state, the loss of fluid by drainage per unit length is uniform along the current.

Again, a series of numerical experiments confirms that the flow evolves to this solution from a range of initial conditions. Figure 5 illustrates the development to the steady-state solution for $\epsilon = 0.2$, from a triangular initial condition. The profile remains approximately linear throughout, with the gradient evolving rapidly towards the analytical value; the volume per unit width of the current then evolves more slowly towards the analytical solution.

2.4. *Axisymmetric flows*

It is also possible to construct the model in an axisymmetric geometry. Again, we assume hydrostatic pressure (equation (2.1)), and a transport velocity modelled by Darcy's law (equation (2.3)). The continuity equation in an axisymmetric geometry has the form

$$\phi\frac{\partial h}{\partial t} + \frac{1}{r}\frac{\partial}{\partial r}(ruh) = -v, \tag{2.29}$$

where r is the radial coordinate in the horizontal plane, and $v(r,t)$ is the vertical drainage velocity through the underlying layer. For an intrusion of volume $\mathcal{V}_{\mathrm{a}}$, the global volume condition has the form

$$\lim_{t\to 0}\int_0^{R(t)} 2\pi r h(r,t)\,\mathrm{d}r = \mathcal{V}_{\mathrm{a}}. \tag{2.30}$$

2.4.1. *Finite-volume release*

We combine the expressions for pressure, velocity and continuity as before, and we introduce dimensionless variables

$$\hat{r} = r\left(\frac{2\pi}{\mathscr{V}_\mathrm{a}}\right)^{-1/3}, \quad \hat{t} = t\beta\left(\frac{2\pi}{\mathscr{V}_\mathrm{a}}\right)^{1/3}, \quad \hat{h} = h\left(\frac{2\pi}{\mathscr{V}_\mathrm{a}}\right)^{-1/3}, \tag{2.31}$$

where β is defined as in equation 2.5, to obtain

$$\frac{\partial \hat{h}}{\partial \hat{t}} = \frac{1}{\hat{r}}\frac{\partial}{\partial \hat{r}}\left(\hat{r}\hat{h}\frac{\partial \hat{h}}{\partial \hat{r}}\right) - \hat{v} \quad \text{and} \quad \lim_{\hat{t}\to 0}\int_0^{\hat{R}(\hat{t})} \hat{r}\hat{h}(\hat{r},\hat{t})\,\mathrm{d}\hat{r} = 1. \tag{2.32}$$

As before, the draining term is $\hat{v} = 0$ for an impermeable bed, $\hat{v} = K_b\mathscr{V}_\mathrm{a}^{1/3}/(2\pi K b) = \lambda_\mathrm{a}\hat{h}$ for gravity-driven drainage, and $\hat{v} = w/\beta = \epsilon$ for drainage driven by an imposed vertical flow.

In the case of an impermeable bed, equation (2.32) admits a similarity solution,

$$\hat{h}(\hat{r},\hat{t}) = \tfrac{1}{8}\hat{t}^{-1/2}\left[\eta_N^2 - \frac{\hat{r}^2}{\hat{t}^{1/2}}\right]. \tag{2.33}$$

where $\eta_N = 2^{5/4}$.

For gravity-driven drainage, $\hat{v} = \lambda_\mathrm{a}\hat{h}$, we can apply the transformation (2.15) to recover the equation

$$\frac{\partial H}{\partial \tau} = \frac{1}{\hat{r}}\frac{\partial}{\partial \hat{r}}\left(\hat{r}H\frac{\partial H}{\partial \hat{r}}\right), \tag{2.34}$$

which has the solution

$$\hat{h}(\hat{r},\hat{t}) = \tfrac{1}{8}e^{-\lambda_\mathrm{a}\hat{t}}\left(\frac{1-\exp(-\lambda_\mathrm{a}\hat{t})}{\lambda_\mathrm{a}}\right)^{-1/2}\left[\eta_N^2 - \hat{r}^2\left(\frac{1-\exp(-\lambda_\mathrm{a}\hat{t})}{\lambda_\mathrm{a}}\right)^{-1/2}\right]. \tag{2.35}$$

For drainage driven by background flow, $\hat{v} = \epsilon$, there is again an exact solution,

$$\hat{h}(\hat{r},\hat{t}) = \tfrac{1}{8}\hat{t}^{-1/2}\left[\eta_N^2 - \frac{\hat{r}^2}{\hat{t}^{1/2}}\right] - \tfrac{2}{3}\epsilon\hat{t}, \tag{2.36}$$

and we note that this can be rewritten in the form

$$\begin{aligned}\hat{h}(\hat{r},\hat{t}) &= \tfrac{1}{8}\hat{t}^{-1/2}\left[\eta_N^2 - \tfrac{2}{3}\epsilon\hat{t}^{3/2}\right](1-\zeta^2)\\ &= \hat{h}(0,\hat{t})(1-\zeta^2),\end{aligned} \tag{2.37}$$

where $\zeta = \hat{r}/\hat{R}(\hat{t})$, and the dimensionless radius of the current is

$$\hat{R}(\hat{t}) = \sqrt{\eta_N^2\hat{t}^{1/2} - \tfrac{16}{3}\epsilon\hat{t}^2}. \tag{2.38}$$

These solutions have been reproduced by numerical integration of equation (2.32) for a finite-volume release from various initial conditions, which indicates that they are stable and suggests that they act as an intermediate asymptotic in the same manner as the planar solutions.

2.4.2. *Steady-flow solutions*

It is also interesting to seek steady-state solutions, which correspond to the states which might evolve, for example, due to constant injection of fluid from a vertical pipe inserted at $r = 0$. The flux of volume per unit time is denoted by $\mathscr{Q}_\mathrm{a}$, and after

combining the continuity and Darcy equations in the usual way and scaling by the length scale $[\mathcal{Q}_a/(2\pi\beta)]^{1/2}$, we obtain the equation

$$\frac{\partial}{\partial\hat{r}}\left(\hat{r}\hat{h}\frac{\partial\hat{h}}{\partial\hat{r}}\right) = \hat{v}\hat{r}, \tag{2.39}$$

where, for drainage driven by an external flow, $\hat{v} = \epsilon$ as before; and for gravity-driven drainage, $\hat{v} = h[K_b\mathcal{Q}_a^{1/2}/(2\pi\beta^{1/2}Kb)]$. The boundary condition at the origin is

$$\lim_{\hat{r}\to 0}\left(\hat{r}\hat{h}\frac{\partial\hat{h}}{\partial\hat{r}}\right) = -1. \tag{2.40}$$

In the case of flow-driven drainage, $\hat{v} = \epsilon$, we have a simple condition for global mass balance, $\epsilon\hat{R}^2 = 2$, and we can obtain the analytical solution

$$\hat{h}(\hat{r}) = \sqrt{\tfrac{1}{2}\epsilon\hat{r}^2 - 2\log(r\sqrt{\tfrac{1}{2}\epsilon}) - 1}. \tag{2.41}$$

We note that this profile becomes singular at $\hat{r} = 0$, although the flux is bounded.

In the case of gravitationally driven drainage, we have been unable to obtain an analytical solution, although equation (2.39) can be integrated numerically in the region away from $r = 0$.

3. Initial conditions and adjustment

Much of the motivation for developing similarity solutions comes from their role as intermediate asymptotic solutions (Barenblatt 1996). Although the similarity solutions have a highly idealized singular initial condition, they describe the behaviour of the system as it evolves from a much wider range of initial conditions, for times large enough that the details of the initial state have been lost, but before the system reaches its long-term equilibrium. For non-draining gravity currents in the laboratory, the flow has typically 'forgotten' the initial conditions, and adjusted to a self-similar form, once it has travelled a few times the length of the initial release (the so-called 'lock-lengths rule').

It seems reasonable to hope that our analytical solutions will play the same role for draining flows. However, there may be initial conditions which are so far from the analytical solution that the flow is unable to adjust to it before the fluid has drained out entirely; and there are certainly initial conditions which will be longer than the run-out length of the analytical solution. In discussing the relevance of our solutions, therefore, it is important to quantify both the length scales and time scales of the adjustment process and the regimes of initial conditions in which adjustment is impossible.

This is not a question of merely mathematical interest. In natural or industrial situations, the initial distribution of fluid will have finite depth and lateral extent, and in laboratory experiments, fluid is typically released from a lock of finite length. Thus, if we hope to test our models experimentally or to use them to make quantitative predictions, we must take account of the adjustment process.

In order to investigate these issues, we have integrated the dimensionless governing equations (2.7), (2.14) and (2.23) numerically, for a range of initial conditions. First we describe the behaviour of non-draining flows (§ 3.1), then we move to the draining

flows (§§ 3.2, 3.3). For notational convenience, the hats on all dimensionless variables have been dropped for the remainder of this section.

In order to describe the convergence of our numerical solutions to the analytical solutions, we require a means to quantify the shape of the current profiles. The analytical solutions for a finite release of fluid, (2.8), (2.17), (2.26), can all be written in the form $h(0,t)m(\zeta)$, for $\zeta = x/L(t)$, and so the volume of fluid per unit width may be written in the form

$$V(t) = \int_0^{L(t)} h(x,t)\,\mathrm{d}x = L(t)h(0,t)\int_0^1 m(\zeta)\,\mathrm{d}\zeta. \tag{3.1}$$

Therefore, for all the analytical solutions, the shape factor $\Gamma(t)$ defined by $\Gamma(t) \equiv V(t)/[h(0,t)L(t)]$ is constant in time, and in each case it has value $2/3$. In contrast, if the fluid is released from a rectangular initial distribution with volume per unit width 1, $\Gamma(0) = 1$, while for a triangular initial distribution, with apex at $x = 0$, $\Gamma(0) = 1/2$.

This suggests that, by following the evolution of $\Gamma(t)$ from an arbitrary initial condition, we may examine the shape evolution of the current. As the current adjusts to the analytical solution, $\Gamma(t) \to 2/3$ as time increases, and we can define the degree to which the current has adjusted as $|\Gamma(t) - 2/3|$. The use of $\Gamma(t)$ to track the evolution of the current also has the advantage that it makes no prior assumption about the solution (referred to as the target solution) to which the current will converge.

Although the numerical integrations were started from $t = 0$, it is probable that the target solution will have a virtual origin in time at $t = -t_0$, which corresponds to the time at which the length of the target solution vanishes. Furthermore, for draining flows, there will also be a virtual initial volume per unit width, V_0, which corresponds to the volume per unit width of the target solution at $t = -t_0$ (see § 3.3). In other words, rather than converging to the analytical solution $h(x,t;V(0) = 1)$, the current may converge to an analytical solution $h(x,t+t_0;V(-t_0) = V_0)$. The definition of convergence in terms of $\Gamma(t)$ allows us to deduce these quantities from the ones which characterize the convergence process, namely, the time t_{adj} taken to converge to the target solution, the length L_{adj} of the current when convergence has occurred, and the volume per unit width V_{adj} of the current at this time.

In all our numerical experiments, unless otherwise stated, the initial condition was a rectangle of length L_0 and area 1. We find that $\Gamma(t)$ does decrease towards $2/3$, and we regard convergence as corresponding to situations where Γ approaches $2/3$ asymptotically. For convenience, the current was taken to have adjusted to the anaytical solution when $|\Gamma(t) - 2/3| < 0.015$.

3.1. *Impermeable base (no drainage)*

First, we consider a current propagating without drainage. In this case, the convergence to the target solution can be characterized by two quantities, t_{adj} and L_{adj}, while the target solution itself can be characterized by one, t_0. Since t_0 is determined from t_{adj} and L_{adj} using $L(t_{\mathrm{adj}} + t_0) = L_{\mathrm{adj}}$, there are only two independent quantities involved: in fitting the scalings below, this was taken into account.

Numerical experiments were conducted for a range of values of L_0, $0.2 \leqslant L_0 \leqslant 4.0$. It was found empirically that $t_0 = (0.225 \pm 0.002)L_0^3$, $L_{\mathrm{adj}} = (1.64 \pm 0.04)L_0$ and $t_{\mathrm{adj}} = (0.265 \pm 0.04)L_0^3$. The functional form of these scalings may be expected, because L_0 is the only free parameter in the initial conditions, and according to the similarity solution, the current length evolves as $t^{1/3}$.

For illustration, profiles of the height of the current are shown in figure 6 for a numerical calculation with initial condition $L_0 = 3.0$.

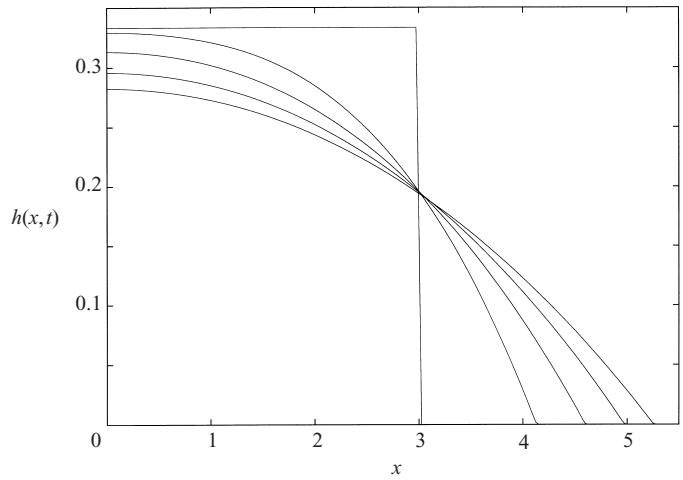

FIGURE 6. Convergence to similarity solution from a rectangular initial condition, $L_0 = 3.0$: height of the current $h(x,t)$ as a function of position, x, at $t = 0$, 2.5, 5, 7.5, 10 ($\Gamma \approx 1$, 0.74, 0.7, 0.68, 0.67 respectively)

Numerical calculations were also carried out for the same range of L_0, from a triangular initial condition, of initial length L_0 and height $2/L_0$ at $x = 0$. The corresponding (empirical) results were: $t_0 = (0.0887 \pm 0.001)L_0^3$; $L_{\mathrm{adj}} = (1.25 \pm 0.03)L_0$; and $t_{\mathrm{adj}} = (0.128 \pm 0.005)L_0^3$. The results for both the rectangular and triangular initial conditions suggest that the 'lock-length' rule of thumb is valid, since the current has adjusted to self-similar form before it has travelled more than two lock lengths.

3.2. *Gravity-driven drainage*

In the various physical contexts where a current both spreads and drains (such as the spread of injectate through an oil reservoir, or of pollutants through an aquifer), one of the most important quantities is the run-out length $L_{\max}$ of the current. For gravity-driven drainage, this coincides with $L_\infty \equiv \lim_{t\to\infty} L(t)$, since the current does not recede.

It is useful to be able to predict the run-out length from the initial length L_0. We expect that in the regime of very small L_0, the current propagates according to the analytical solution 2.17, while in the regime of very large L_0, the current propagation approximates that corresponding to the Heaviside problem described in Appendix B. In order to obtain estimates of $L_{\max}$ for intermediate initial conditions, it is necessary to consider the adjustment process in some detail. This will allow us both to characterize the target solution and to define the regime in which adjustment does occur.

We note that it is possible to scale λ out of the problem altogether using the transformed variables $t' = \lambda^{2/3}t$, $h' = \lambda^{-1/3}h$, $x' = \lambda^{1/3}x$. This suggests that the critical parameter which distinguishes between adjusting and non-adjusting regimes will be $\lambda^{1/3}L_0$.

As discussed in § 2.2, the motion of a speading current which drains under gravity can be described by the same equation as a non-draining current by using a modified time coordinate $\tau = [1 - \exp(-\lambda t)]/\lambda$ in place of t. We therefore expect some correspondence between the two kinds of flow. In particular, the adjustment is still characterized by two quantities, τ_{adj} and L_{adj}, and the target solution can still be

described by a single parameter, τ_0. We note from (2.13), however, that the target solution must also have an 'initial' volume per unit width $V_0 = \exp(\lambda t_0) = (1-\lambda\tau_0)^{-1}$, in order that the volume per unit width as well as the length of the analytical solution coincides with that of the current at $t_{\rm adj}$.

An immediate consequence is that the run-out length, L_∞, can be evaluated as a function of τ_0,

$$L_\infty = \left(\frac{9V_0}{\lambda}\right)^{1/3} = \left(\frac{9}{\lambda(1-\lambda\tau_0)}\right)^{1/3}. \tag{3.2}$$

The situation is further complicated by the fact that τ only reaches a finite limit $1/\lambda$ as $t \to \infty$. Consequently, if the initial distribution of fluid requires a time $\tau_{\rm adj} > 1/\lambda$ to adjust, then the flow will not fully converge to the analytical solution before it has all drained away.

Numerical calculations were carried out, starting from a rectangular initial condition of volume per unit width 1, with length L_0 in the range 0.5 to 5.0, and with the parameter λ taking values in the range 0.02 to 0.5. For each experiment, the quantities $t_{\rm adj}$ and $L_{\rm adj}$ were measured, and t_0 was determined from these by fitting $L(t+t_0) = L_{\rm adj}$.

The results for cases where convergence did occur are rather similar to those for the non-draining case:

$$\tau_0 = (0.21 \pm 0.015)L_0^3, \quad L_{\rm adj} = (1.69 \pm 0.01)L_0, \quad \tau_{\rm adj} = (0.32 \pm 0.02)L_0^3. \tag{3.3}$$

Our scaling estimate for $\tau_{\rm adj}$ allows us to obtain an upper bound for the region where it is possible for convergence to occur. As $t \to \infty$, $\tau \to 1/\lambda$, and so for convergence we require $\tau_{\rm adj} < 1/\lambda$, or, approximately, $\lambda L_0^3 < 3.13$. This is a stronger convergence criterion than that supplied by $L_0 < L_\infty(\lambda)$, which, using our empirical result for $V_0(\lambda)$, corresponds to $\lambda L_0^3 < 4.76$. This is to be expected: in the latter case we merely stipulate that the initial length be less than the maximum possible run-out length of the analytical solution, while in the former case, we allow for the increase in length as the current slumps towards the analytical form. We note, however, that this criterion is still only an upper bound. It depends on the choice of δ such that $|\Gamma - 2/3| < \delta$ defines complete adjustment, and we may expect that for λL_0^3 close to 3.13, estimates for L_∞ based on the assumption of complete adjustment will become inaccurate. (This can be observed in figure 10, where the estimate becomes poor for $\lambda^{1/3}L_0 > 1$.)

The evolution of the current profile is illustrated in figures 7 and 8, which show, respectively, the case $\lambda = 0.1$, $L_0 = 3.0$ for which the current does adjust to the analytical solution, and the case $\lambda = 0.1$, $L_0 = 5.0$ for which the current does not adjust. The most obvious difference is to be seen near the tail of the current: in the non-converging case, the tail is much flatter. In figure 9, $\Gamma(t)$ is plotted for the same currents.

In the regime of very large L_0, the run-out length is dominated by the initial length, and an argument considering the Heaviside problem (see Appendix B) suggests that $L_\infty \sim L_0 + 1.238(L_0\lambda)^{-1/2}$. This estimate is in accord with the results of numerical runs for values of $L_0\lambda^{1/3}$ as small as about 1, even though the model is only strictly valid for large values of $L_0\lambda^{1/3}$.

In figure 10, the scaled quantity $\lambda^{1/3}L_\infty$ is plotted as a function of $\lambda^{1/3}L_0$, for various λ. We compare this with a semi-empirical result $L_\infty = (9/\lambda(1 - 0.21\lambda L_0^3))^{1/3}$, which is derived by substituting our empirical scaling for τ_0, equation (3.3), into equation (3.2), and with the numerically derived asymptotic result $L_\infty \sim L_0 + 1.238/(\lambda L_0)^{1/2}$ for large $L_0\lambda^{1/3}$. The estimates are seen to provide a very good description in their

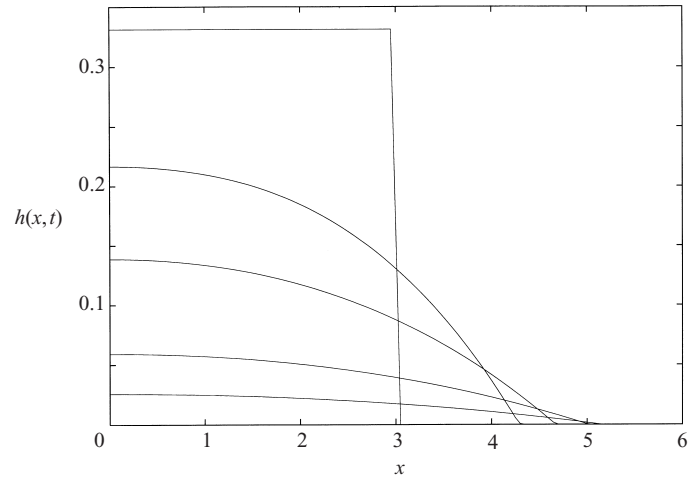

FIGURE 7. Gravity-driven drainage with $\lambda = 0.1$, $L_0 = 3.0$: profiles of the current, h, as a function of x, at $t = 0$, 4, 8, 16, 24 ($\Gamma \approx 1$, 0.72, 0.69, 0.68, 0.67 respectively).

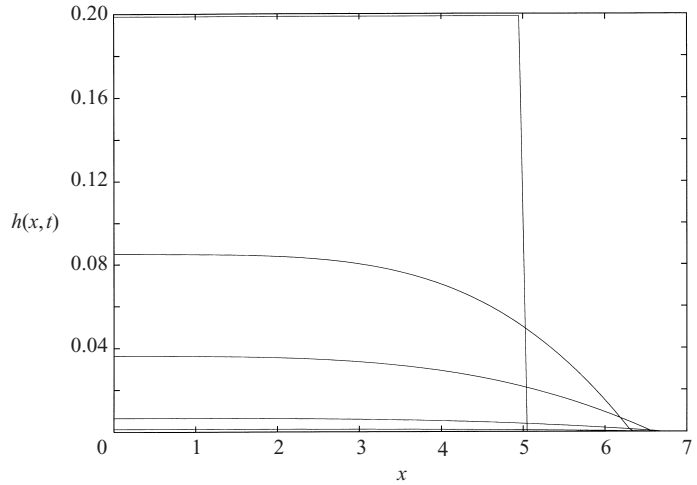

FIGURE 8. Gravity-driven drainage with $\lambda = 0.1$, $L_0 = 5.0$: profiles of the current at $t = 0$, 8.5, 17, 34, 50 ($\Gamma \approx 1$, 0.79, 0.76, 0.75, 0.75 respectively).

respective regimes. Hence, for any initial length of release, we have a simple estimate of the maximum runout.

3.3. *Drainage driven by background flow*

The situation in which the drainage is driven by a background flow is rather more complicated. There are two main differences from the case of gravity-driven drainage. First, it cannot be mapped to the non-draining problem as it could in § 3.2. Secondly, the run-out length, $L_{\max}$, no longer corresponds to the long-time limit L_∞: rather, the current reaches a maximum length in a finite time, before retreating and eventually draining out entirely.

Our object is again to determine how the maximum extent of the current, $L_{\max}$, varies with L_0. In order to do this, we must consider the adjustment process in some detail. There are now three quantities which characterize the convergence: $t_{\rm adj}$, $L_{\rm adj}$

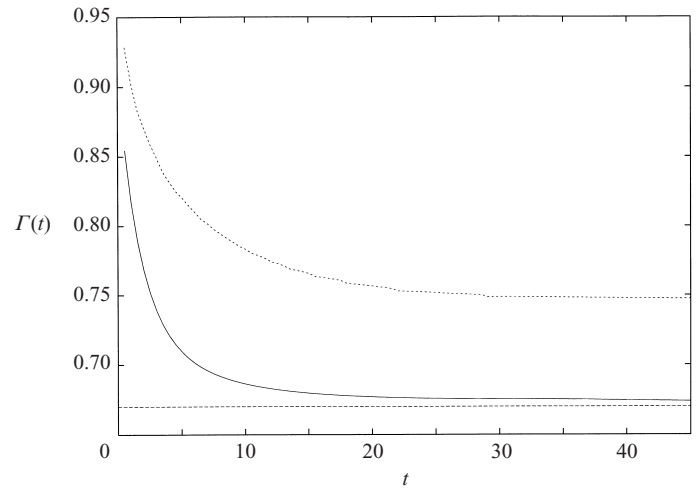

FIGURE 9. $\Gamma(t)$ for the cases $\lambda = 0.1$ and: —, $L_0 = 3.0$ (adjustment occurs); · · · · ·, $L_0 = 5.0$ (adjustment does not occur). Note that in the second case, $\Gamma(t)$ tends to a limit $\neq 2/3$. This is the value that $\Gamma(\tau)$ has reached by $\tau = 1/\lambda$; the value is different from $2/3$ for currents which do not converge to the analytical solution $\Gamma = 2/3$.

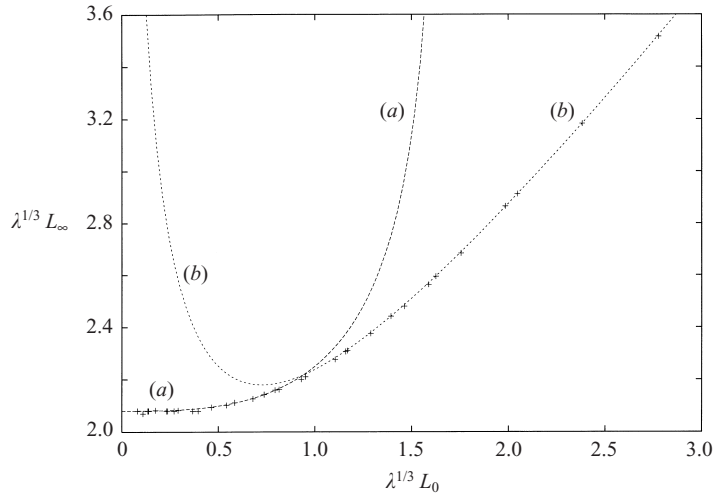

FIGURE 10. The scaled run-out length $\lambda^{1/3}L_\infty$ as a function of $\lambda^{1/3}L_0$ for $\lambda = 0.5, 0.2, 0.1, 0.05, 0.02$: numerical results (+) compared with semi-empirical (curve a) and asymptotic (curve b) results.

and V_{adj}; and two which characterize the target solution: t_0 (as before); and V_0, the virtual initial volume parameter, which cannot now be expressed as a function of t_0 alone.

We note that it is possible to scale ϵ out of the problem by transforming to variables $t' = t\epsilon^{3/4}$, $x' = x\epsilon^{1/4}$ and $h' = h\epsilon^{-1/4}$, and that the critical parameter will therefore be $\epsilon^{1/4}L_0$.

Numerical calculations were carried out for a range of values of ϵ from 0.001 to 0.2, for a rectangular initial distribution of fluid, with L_0 ranging between 0.5 and 8.0. The evolution of the currents was followed until the point when $|\Gamma(t) - 2/3| < 0.015$, as before.

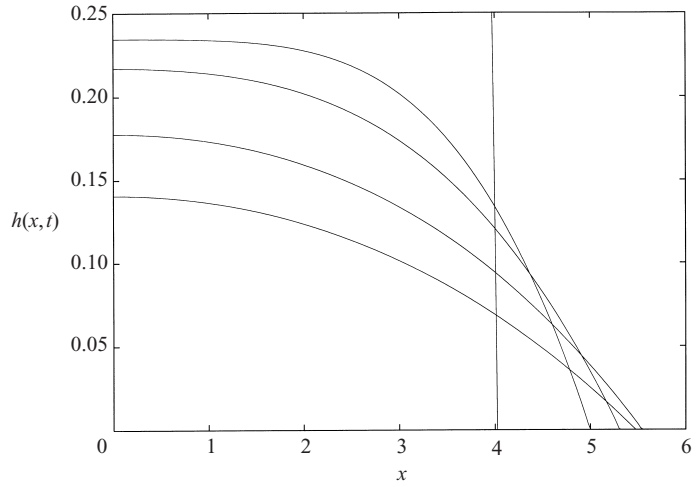

FIGURE 11. The evolution of the current from a rectangular initial condition when drainage is driven by a background flow ($L_0 = 4.0$, $\epsilon = 0.005$): profiles of the current at $t = 0$, 3, 6, 12, 18 ($\Gamma \approx 1.0$, 0.79, 0.74, 0.7, 0.68 respectively)

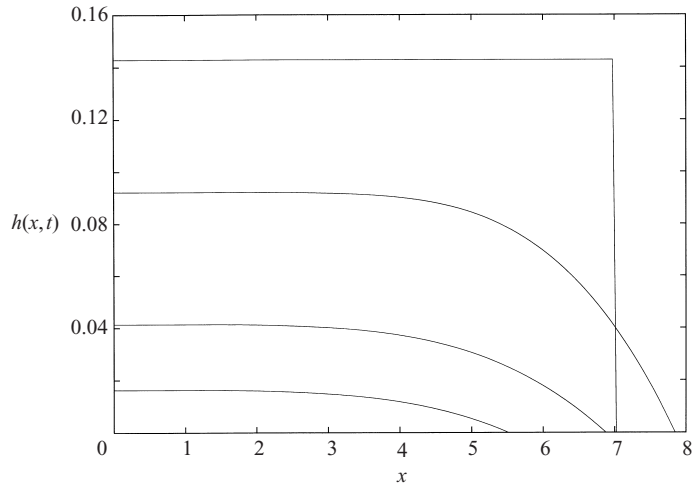

FIGURE 12. The evolution of the current from a rectangular initial condition when drainage is driven by background flow ($L_0 = 7.0$, $\epsilon = 0.005$): profiles of the current at $t = 0$, 10, 20, 25 ($\Gamma \approx 1.0$, 0.84, 0.81, 0.8 respectively). Note that in this case, convergence does not occur.

Figures 11 and 12 illustrate the evolution of currents which, respectively, do and do not adjust to the analytical solution before draining out entirely. As in § 3.2, it is evident that the tail of the current is much flatter in the non-adjusting case, since the change of shape has not fully diffused back from the nose.

It was not possible to obtain simple expressions, analagous to equations (3.3), for the adjustment parameters L'_{adj} and t'_{adj}. Figure 13 shows the quantity L'_{adj} plotted as a function of L'_0, along with the empirical result $L_{\mathrm{adj}} = 1.64L_0$ for the non-draining case. This plot illustrates why adjustment and run-out length in this case are harder to describe than in the case of gravitationally driven drainage: for sufficiently large

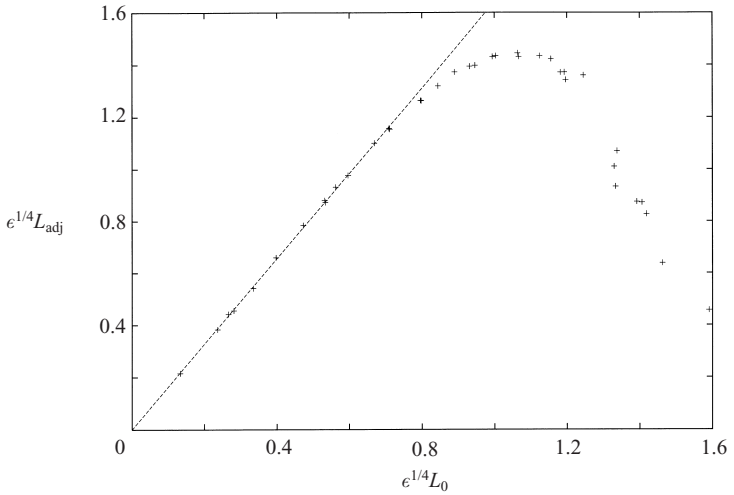

FIGURE 13. $\epsilon^{1/4}L_{\rm adj}$ plotted as a function of $\epsilon^{1/4}L_0$, with $L_{\rm adj} \sim 1.64L_0$ also shown.

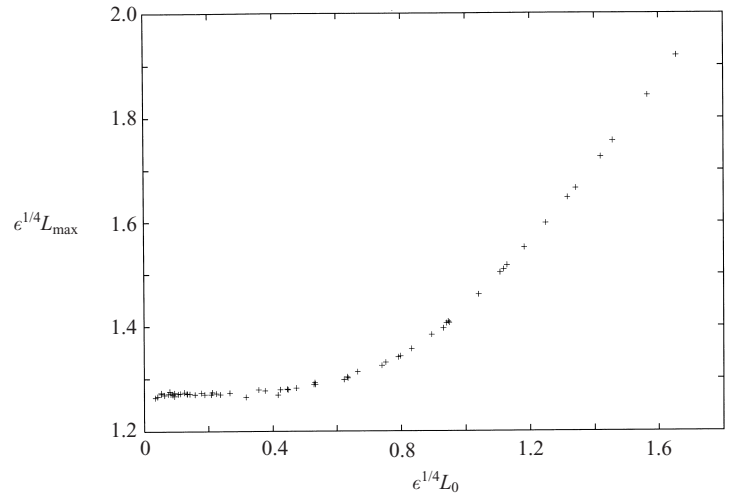

FIGURE 14. $\epsilon^{1/4}L_{\rm max}$ as a function of $\epsilon^{1/4}L_0$ for $\epsilon = 0.05, 0.04, 0.03, 0.02, 0.01, 0.005, 0.002, 0.001$.

values of L_0', the nose of the current is retreating by the time it has adjusted, and the analytical solution is useless in predicting $L_{\rm max}'$.

In figure 14, $L_{\rm max}'$ is plotted as a function of L_0': as before, the data are taken for a range of ϵ between 0.001 and 0.2. In the regime $L_0' \ll 1$, the current converges almost instantaneously to the analytical solution with $V_0 = 1$, and so $L_{\rm max} \approx 1.278\epsilon^{-1/4}$. The constant in this relation, $(8/3)^{1/4} \approx 1.278$, is obtained from the analytical solution, equation (2.25).

Considering the regime in which $L_0' \gg 1$, it is intuitively clear that the run-out length will be dominated by the initial length, and that, the longer and thinner the current, the less opportunity it will have to spread before draining entirely: this allows us to obtain an asymptotic bound for $L_{\rm max}$ in the regime $L_0' \gg 1$. First we note that the time before the current drains out entirely is smaller than $(L_0\epsilon)^{-1}$, and the maximum distance it could advance in that time is given approximately by $1.238L_0^{-1/2}(L_0\epsilon)^{-1/2}$

(see Appendix B). This allows us to make the estimate $L_{\max} \leqslant L_0 + 1.238\epsilon^{-1/2}L_0^{-1}$ for large L_0'. In fact, for all our data, this upper bound is a considerable overestimate for $L_{\max}$. It is likely that our data, which only extend to $\epsilon^{1/4}L_0 \approx 1.7$, simply do not reach the regime where the asymptotic result is a good approximation.

3.4. *Comments on the generality of our solutions*

The main conclusion to be drawn from this series of numerical experiments is that there is an important difference between our analytical solutions for draining currents and the similarity solutions for non-draining currents. While our solutions are attracting, in the sense that a flow will adjust towards them from more general initial conditions, the adjustment time may exceed the time taken for the current to drain out entirely. Hence our solutions can only be regarded as intermediate asymptotics for a restricted range of initial conditions, and only in this regime can they be used to predict quantities such as run-out length.

4. Experiments

Motivated by the model results, we have conducted a series of experiments which examine the motion of gravity currents through a Hele-Shaw cell with a small gap at the base. This provides an analogue experimental system for modelling gravity-driven flow through a layer of permeable rock underlain by a layer of lower permeability, with a permeable lower boundary. The cell had height 30 cm and length 50 cm, with a gap width of 9 mm, corresponding to an effective permeability of 6.75 mm^2. The permeable lower boundary had a gap width of 3 mm, corresponding to an effective permeability of 0.75mm^2, and was 21 mm deep.

We examined the spreading into air of finite-volume currents of golden syrup, released from a rectangular source located behind a lock gate. Although the viscosity of golden syrup is highly temperature-dependent, the time taken for the experiments was sufficiently short (of the order of 5 minutes) that the room temperature could be regarded as constant. Estimates of the fluid density ($\approx 1400\,\mathrm{kg\,m^{-3}}$) and the viscosity ($\approx 20\,\mathrm{kg\,m^{-1}\,s^{-1}}$) give Reynolds numbers of the order of 10^{-3} to 10^{-2} for these experiments.

Figure 15 shows photographs of the current which illustrate its development as it spread and drained. The length $L(t)$ of the current was recorded at regular intervals.

There are two simple tests we can make of the model. First, the run-out length $L_\infty = (9\nu K b/K_b)^{1/3}$ does not depend on the fluid viscosity, and can be compared with the actual distance reached by the experimental current. It can be seen from table 1 that the theoretical prediction is reasonably accurate, although it systematically overestimates the actual run-out length. This is discussed below. Secondly, we consider the quantity $\log\,[1-(L(t)/L_\infty)^3]$, which is plotted in figure 16. Equation (2.18) suggests that this should decrease linearly with time, and it can be seen from the figure that this is a good description for at least the main part of the motion, after the current has adjusted to a self-similar form but before it reaches its full run-out length.

The main difference between the behaviour of the experimental current and that predicted by our model comes at large times, as the experimental current comes to rest at a run-out distance $L_{\max} < L_\infty$. This may be largely due to the finite depth of the lower boundary, which was not fully saturated with fluid near the nose of the current, leading to an effectively smaller value of b and thus to increased drainage near the nose and a reduced run-out length. Another effect which is not accounted for in our model is that of basal drag, which may be expected to become significant

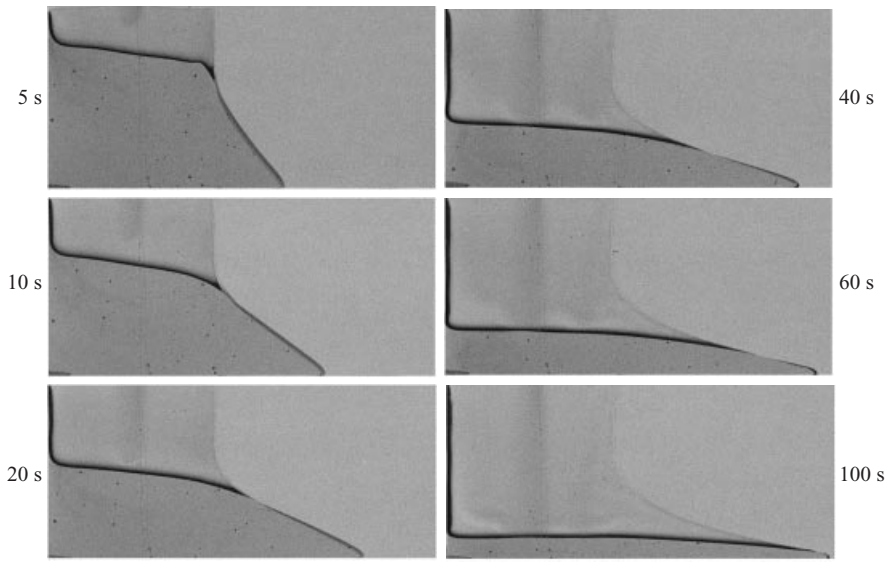

FIGURE 15. Sequence of photographs of the experiment described in § 4, illustrating the evolution of the shape of an experimental current. The photos were taken 5, 10, 20, 40, 60 and 100 s after the release. Some capillary effects are evident at the 'tail' of the current.

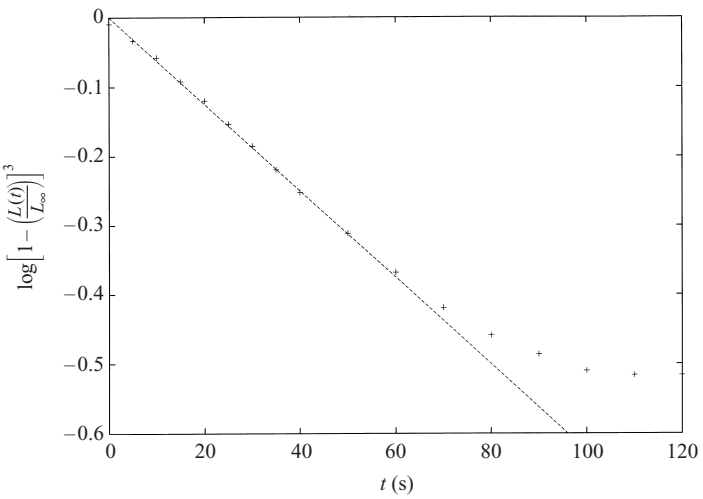

FIGURE 16. Experimental results: $\log(1-(L(t)/L_\infty)^3)$ plotted as a function of time, together with linear best-fit line. Between 0 and 10 s, there is some evidence of adjustment, and after about 80 s, the current is slowed by capillary effects and enhanced drainage (see text for details).

when the depth of the current is comparable with the width of the cell. The effect of capillary forces can also be seen near the nose of the current, where there is a tendency for the interface to form an obtuse (rather than an acute) angle with the base of the cell.

Despite the divergence from the model solution at long times, the results of our preliminary experiments are encouraging and support the present modelling approach. We hope to be able in the future to carry out a more thorough experimental

Length × height of lock (mm × mm)	L_{max} (actual) (mm)	L_∞ (theoretical) (mm)	L_{max}/L_∞
100 × 92	231	265	0.92
100 × 100	231	273	0.90
100 × 110	228	281	0.86
100 × 197	281	342	0.87
75 × 150	237	267	0.89
100 × 150	254	294	0.86

TABLE 1. Run-out length compared with theoretical predictions for various volumes of the initial release.

investigation, varying parameters such as viscosity of the fluid and the widths both of the cell and of the gap at the base.

5. Application to some physical situations

Although the drainage effects we have considered involve flows which are of small magnitude compared to the horizontal spreading of the current, their effect on the behaviour of the current can be significant. To illustrate this, we apply our model for a planar, gravity-driven draining flow to the dispersal of contaminant and tracers through an aquifer, and we apply our model for a particle-laden current spreading in a fracture to the injection of propants into a fractured oil reservoir. In each case, our analysis indicates that drainage effects are important over time scales of industrial relevance.

5.1. *Dispersal in an aquifer*

It is difficult to obtain detailed information about the permeability structure of a porous rock in its natural setting. Industries interested in flow through such permeable rocks often conduct experiments in which tracer is injected in one well, and the outflow from other wells is then monitored to determine the time and concentration of tracer which re-surfaces at the environment. Hence it is possible to estimate the effective bulk permeability of the rock. However, this study indicates the care with which such data should be interpreted.

Many aquifers involve layers of different and sharply contrasting permeability. If some contaminant or tracer is injected at one well, it is likely that the injected fluid will be of different density to the host fluid, owing to differences in temperature and natural dissolved minerals in the ambient fluid. The injectate will therefore tend to spread out from the injection well, and once it has spread far enough, the motion will be dominated by buoyancy forces (see e.g. Woods & Mason 2000). Initially the injectate will tend to spread along the high-permeability layer, but if there is an underlying lower-permeability layer, then, as it spreads laterally, the tracer will gradually drain away. The effect of such drainage is to slow the lateral spreading of the tracer, and it may ultimately arrest this motion, so that all the tracer drains into a lower part of the formation.

For illustration, we present a model calculation in which we examine the gravitational dispersal of a contaminant injected into an aquifer. We assume that a volume $\mathscr{V}_a$ of $1\,m^3$ is injected at some initial time into a layer with permeability $10^{-12}\,m^2$. We also assume that the lower boundary of this layer has permeability $10^{-14}\,m^2$, and

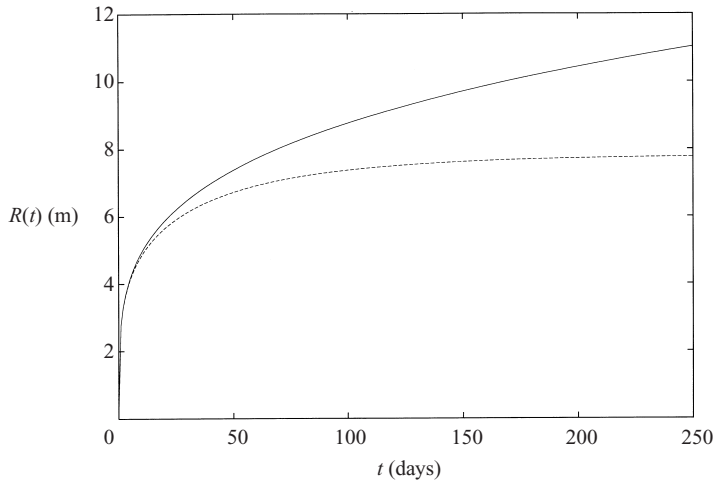

FIGURE 17. The distance propagated by the current, $R(t)$, as a function of time, for flow in an aquifer: solid line is non-draining, dashed line draining case.

thickness 0.1 m, which is representative of some layered sandstones. In this case, the parameter λ_a takes the value $\lambda_a = 10^{-1}$. Assuming that the reservoir is laterally extensive, and that the buoyancy of the injected water has reduced gravity $g' = 0.1\,\mathrm{m\,s^{-2}}$, corresponding to a small difference in dissolved mineral content between the injected and host fluids, then the parameter β has value $\beta = 10^{-6}\,\mathrm{m\,s^{-1}}$. Figure 17 illustrates the distance the current will spread, in dimensional units, as a function of time, for the case in which we account for the permeability and drainage into the lower layer and the case in which we do not, following the analysis for an axisymmetric current in § 2.4. We infer from this figure that, even if the lower boundary of the layer has very small permeability compared to the main flow channel, the draining arrests the propagation of the flow substantially after times of order $\mathscr{V}_a^{1/3}/(\beta\lambda_a) \approx 10^7\,\mathrm{s}$ (≈ 100 days) in comparison to the case in which the lower layer is impermeable.

5.2. *Particle injection in a fracture*

A second process for which the present analysis has some relevance concerns the dispersal of particle-laden fluid through fractures. For example, particle-laden fluid is sometimes injected into oil reservoirs to hold open the fracture and maintain relatively high-permeability flow paths (e.g. Pearson 1984). The actual process is highly complex, owing to the different constituent fluids involved. In order to gain some insight into part of the process, it is of interest to examine the effect of particle fallout on the distance over which a gravity-driven flow, whose buoyancy arises from the presence of the particles, may carry the particles. We consider a fracture of width 0.1 m and an ambient fluid of kinematic viscosity $10^{-3}\,\mathrm{m^2\,s^{-1}}$; the injected fluid contains particles with settling velocity $10^{-4}\,\mathrm{m\,s^{-1}}$, the reduced gravity of the suspension is $g' = 0.1\,\mathrm{m\,s^{-2}}$, and the volume of injectate per unit width is of order $1\,\mathrm{m^2}$. In this case, β has a value of order $10^{-1}\,\mathrm{m\,s^{-1}}$ and the parameter ϵ is of order 10^{-3}. From (2.24), we deduce that the particles will spread laterally for a time of order $10^3\,\mathrm{s}$, reaching a maximum distance of order 10 m, before they have settled from the flow. Again, for comparison, we illustrate the propagation distance of the current in the case that the particle settling is neglected in figure 18. In this example, the figure illustrates the importance of the settling in arresting the flow after a time of order 500 s.

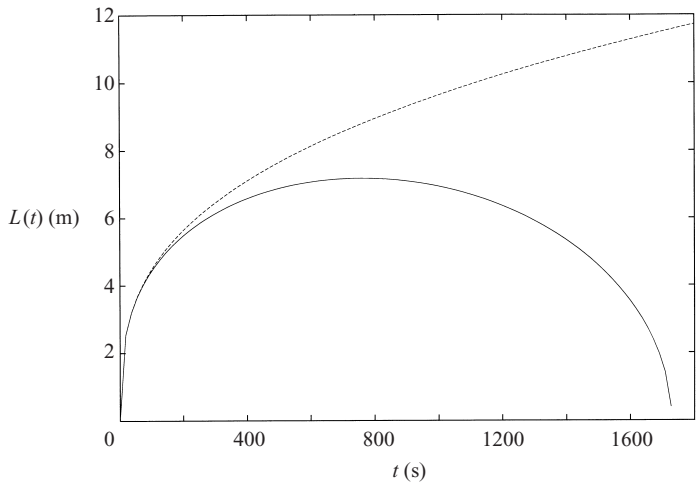

FIGURE 18. The distance propagated by the current, $L(t)$, as a function of time for flow in a fracture, as described in § 5: solid line is sedimenting, dashed line non-sedimenting case.

6. Discussion and conclusion

We have developed a model which describes the propagation of a current of dense fluid through a saturated layered porous medium. We have examined motion along one high-permeability channel, including the effects of drainage through a thin underlying layer of much smaller permeability. The governing partial differential equations were derived in the limit that the current is long and thin, and hence that the pressure is locally hydrostatic.

We have presented exact analytical solutions in both planar and axisymmetric geometries for a fixed-volume release of fluid, in the cases that (i) there is no loss of fluid through the less-permeable layer; (ii) there is a drainage of fluid through the less-permeable layer, driven by hydrostatic pressure in the upper layer; and (iii) there is a drainage of fluid driven by an imposed vertical flow in the ambient fluid. In the first case, the length or radius of the current increases as $t^{1/3}$ (planar geometry) or $t^{1/4}$ (axisymmetric geometry); in the second case, it tends to a run-out length or radius which depends on the volume of the current relative to the thickness of the less-permeable layer, and on the permeability contrast between the two layers; and in the third case, the current advances to a maximum length or radius and then retreats before draining out completely. We have also presented steady-state solutions for cases (ii) and (iii) in which a steady flux at the origin matches the draining flow from a finite region of the high-permeability layer.

These analytical solutions have been reproduced by numerical integration of the governing partial differential equations. These numerical solutions suggest that with arbitrary initial conditions, the flow evolves towards the analytical solutions, when possible. For the case of fixed-volume releases in a planar geometry, this convergence process has been investigated in more detail, using a quantitative measure of convergence. Estimates have been obtained for the time and distance over which convergence takes place, for the parameter regime where convergence is possible, and for the run-out length both in the case where convergence is possible and in the case where the initial distribution of fluid is too long and shallow to converge to the analytical solution. The analytical solution for the planar gravity-driven draining flow has also been compared with some analogue laboratory experiments. Finally, we have

considered the implications of our results for two physical situations: the spreading of an injectate in an aquifer, and the injection of particle-laden fluid into a fracture.

We reiterate that the models developed in this study are simplified, but provide valuable insight into the limiting effects of draining on the propagation of gravity-driven flows in porous rocks and fractures. We plan to continue this work by examining the effects of capillarity and wetting on such draining, gravity-dominated displacement flows. Further possible extensions of this work also include multiple layer systems, where flow in the underlying high-permeability layer, or in a low-permeability layer of non-negligible thickness, must be considered.

We are grateful to Vincent Miele and to Lynne Hatcher for assistance with the experiments described in §4, and to the anonymous referees for some extremely constructive comments on the first version of this paper. D. P. acknowledges support from EPSRC and HR Wallingford Ltd. under an EPSRC CASE studentship. A. J. H. acknowledges support from the Nuffield Foundation (grant reference NUF-NAL).

Appendix A. Numerical method used in §§ 2 and 3

The equations (2.14) and (2.23) were solved numerically on a grid of 250 x-points using a explicit (forward-time, centred-space) finite-element scheme (see Press *et al.* 1992),

$$h_{\rm est} = h_{i,t} + \frac{\Delta t}{2(\Delta x)^2}(h_{i-1,t}^2 - 2h_{i,t}^2 + h_{i+1,t}^2), \tag{A 1}$$

$$h_{i,t+\Delta t} = h_{\rm est} - \epsilon\Delta t \quad \text{or} \quad h_{i,t+\Delta t} = h_{\rm est}(1-\lambda\Delta t), \tag{A 2}$$

where $h_{i,t} \equiv h(i\Delta x, t)$. This scheme is second-order in space and first-order in time. The heuristic criterion for stability of this type of scheme is given in Press *et al.* (1992) as $\Delta t \leqslant \min_j [2(\Delta x)^2/(h_j + h_{j+1})]$, which does not guarantee stability near the nose of the current where h becomes very small: however, no instability was evident in any of our results.

At the nose of the current, the scheme (A 1) was modified to use backward-pointing derivatives, effectively reducing it to first-order accuracy in this region. The drainage terms (A 1) were only applied where $h_{\rm est} \geqslant \epsilon\Delta t$ or $\lambda h_{\rm est}\Delta t$ as appropriate.

The method was tested against the analytical solutions (2.17) and (2.24) for a range of λ and ϵ, and found to be extremely accurate up to times when the current had almost totally (more than 99%) drained out. Very small spurious oscillations in h, of the order of 10^{-5}, tended to occur within two or three grid points of the nose, but these did not affect the rest of the solution.

Appendix B. Gravity-driven draining flow: the Heaviside problem

We consider the problem in transformed variables,

$$\frac{\partial H}{\partial \tau} = \frac{\partial}{\partial x}\left(H\frac{\partial H}{\partial x}\right), \tag{B 1}$$

in the context of a 'Heaviside' initial condition, $H(x,0) = H_0$ for $x < 0$, and $H(x,0) = 0$ for $x \geqslant 0$. Intuitively, this condition should act as a model for the case of a very long, thin initial condition for the current (where we will have $H_0 = 1/L_0$).

By analogy with the case of a linear diffusion problem, we seek a similarity solution in terms of a variable $\xi = x\tau^{-1/2}$: this leads to an ODE in $H(\xi)$. We can then simplify

further by transforming to $\hat{H} = H/H_0$ and $\hat{\xi} = \xi H_0^{-1/2}$, so our governing equation becomes

$$-\frac{1}{2}\hat{\xi}\frac{\mathrm{d}\hat{H}}{\mathrm{d}\hat{\xi}} = \frac{\mathrm{d}^2}{\mathrm{d}\hat{\xi}^2}(\hat{H}^2). \tag{B 2}$$

The equation (B 2) can now be integrated numerically, with the conditions that $\hat{H} \to 1$ as $\hat{\xi} \to -\infty$ and that volume per unit width is conserved,

$$\int_{-\infty}^{0} [1 - \hat{H}(\hat{\xi})]\,\mathrm{d}\hat{\xi} = \int_{0}^{\hat{\xi}_F} \hat{H}(\hat{\xi})\,\mathrm{d}\hat{\xi}, \tag{B 3}$$

where $\hat{\xi}_F$ marks the 'front' of the current.

Numerical integration demonstrates that $\hat{\xi}_F = 1.238$, and thus $\xi_F = 1.238 H_0^{1/2}$. In terms of the gravity-driven draining flow, in which the maximum value of τ is $1/\lambda$, this means that the current will run out beyond $x = 0$ by a distance $\xi_F \lambda^{-1/2} = 1.238(L_0\lambda)^{-1/2}$.

We note that we can also quantify somewhat the condition for the Heaviside problem to be a good model for a rectangular initial condition: we may expect this to be the case when no significant disturbance has reached the 'tail' of the current (at $x = -L_0$ in our coordinates here) by the time the shape has finished evolving; in other words when $L_0 > \xi_0 \lambda^{-1/2}$ for some ξ_0 defining the point on the profile where significant disturbance can be seen. Since $\xi_0 = \hat{\xi}_0 L_0^{-1/2}$ for some $\hat{\xi}$ independent of all other parameters, this leads to the requirement that $L_0 > \hat{\xi}_0^{2/3}\lambda^{1/3}$; numerical results suggest that $\hat{\xi}_0 \approx 1$.

REFERENCES

Barenblatt, G. I. 1996 *Scaling, Self-similarity, and Intermediate Asymptotics.* Cambridge University Press.

Bear, J. 1972 *Dynamics of Fluids in Porous Media.* Elsevier.

Christie, M. & Blunt, M. 1993 How to predict fingering in 3 component flow. *Transport in Porous Media* **12** (3), 207–236.

Davis, S. H. & Hocking, L. M. 1999 Spreading and imbibition of viscous liquid on a porous base. *Phys. Fluids* **11**, 48–57.

Davis, S. H. & Hocking, L. M. 2000 Spreading and imbibition of viscous liquid on a porous base II. *Phys. Fluids* **12**, 1646–1655.

Huppert, H. E. 1986 On the intrusion of fluid mechanics into geology. *J. Fluid Mech.* **173**, 557–594.

Huppert, H. E. & Woods, A. W. 1995 Gravity-driven flows in porous layers. *J. Fluid Mech.* **292**, 55–69.

Lake, L. 1989 *Enhanced Oil Recovery*. Prentice Hall.

Murray, J. D. 1989 *Mathematical Biology*. Springer.

Pattle, R. E. 1959 Diffusion from an instantaneous point source with a concentration-dependent coefficient. *Q. J. Mech. Appl. Maths* **12**, 407–409.

Pearson, J. R. A. 1994 On suspension transport in a fracture: framework for a global model. *J. Non-Newtonian Fluid Mech.* **54**, 503–513.

Press, W. H., Teukolsky, S. A., Vetterling, W. T. & Flanner, B. P. 1992 *Numerical Recipies in Fortran.* Cambridge University Press.

Thomas, L. P., Marino, B. M. & Linden, P. F. 1998 Gravity currents over pororus substrates. *J. Fluid Mech.* **366**, 239–258.

Ungarish, M. & Huppert, H. E. 2000 High-Reynolds-number gravity currents over a porous boundary: shallow-water solutions and box-model approximations. *J. Fluid Mech.* **418**, 1–23.

Woods, A. W. 1999 Liquid and vapour flow in superheated rock. *Ann. Rev. Fluid Mech.* **31**, 171–199.

Woods, A. W. & Mason, R. M. 2000 The dynamics of two-layer, gravity-driven flows in permeable rock. *J. Fluid Mech.* **421**, 83–114.